# Dual-wavelength estimates of X-band radar signal attenuation characteristics in rain


CSU CHILL radar

Sergey Y. Matrosov[1,3], Patrick Kennedy[2], Rob Cifelli[3]

[1]*Cooperative Institute for Research in Environmental Sciences, University of Colorado,Boulder,CO 80309*
[2]*Colorado State University, Fort Collins, Colorado, 80523 USA*
[3]*NOAA, Earth System Research Laboratory, Physical Sciences Division, 325 Broadway, Boulder CO, 80305*
(Dated: 16 July 2014)

## 1 Introduction

An active use of polarimetric meteorological X-band (wavelength $\lambda \approx 3$ cm) radars for quantitative precipitation estimation (QPE) has been increasing for a number of years. Particular interest in measurements at this frequency band is dictated by a relative compactness and low cost of X-band radar systems and also by applicability of some polarimetric retrievals for lower rain rates compared to traditional meteorological radar frequencies at S- ($\lambda \approx$ 10-11 cm) and C-bands ($\lambda \approx 5$ cm) (e.g,, Matrosov et al. 2006). Attenuation of X-band radar signals in rain is, however, significant, thus different schemes need to be applied to correct observed reflectivity factor $Z_e$ (hereafter just reflectivity) and differential reflectivity, $Z_{DR}$.

Attenuation correction schemes usually use either simple differential phase approaches (e.g., Matrosov et al. 2002) or range-profiling type approaches (Bringi et al. 2001; Ryzhkov et al. 2014). Both approaches rely on the relation between horizontal polarization attenuation coefficient, $A_h$, and specific differential phase shift between horizontally and vertically polarized radar returns, $K_{DP}$:

$$A_h = \alpha \bullet K_{DP}^{\ \beta} \tag{1}$$

Modeling (e.g., Matrosov et al. 2002) indicates that at X-band $\beta \approx 1$. Differential attenuation ($A_{DP}$) correction to $Z_{DR}$ measurements assumes the relation:

$$A_{DP} = \gamma \bullet K_{DP}^{\zeta} \tag{2}$$

While modeling shows that this relation may deviate from linear, the corresponding deviation is usually is not very severe and many practical applications for simplicity use $\zeta$=1.

Values of the coefficients $\alpha$ and $\gamma$ are crucial for applications of correction schemes at attenuating radar frequencies (note that the range-profiling attenuation correction approaches relate total attenuation and total propagation phase shift by means of $\alpha$, and assume the exponent in the reflectivity – specific attenuation relations). Often values of $\alpha$ and $\gamma$ are found through theoretical modeling assuming an oblate spheroidal rain drop shape and some drop aspect ratio (i.e., minor-to-major dimension ratio) - size relation. Modeling is performed either for theoretical drop size distributions (DSDs), such as gamma-functions, with widely varying parameters or for experimental distributions measured in situ by disdrometers (e.g., Matrosov 2010). Although the theoretical estimation of the coefficients $\alpha$ and $\gamma$ for attenuating radar frequencies is a valid approach, considerable data scatter in reported theoretical relations exist (e.g., Bringi and Chandrasekar 2001) mainly due to differing drop aspect ratio model and DSD assumptions.

For future practical applications, it is desirable to get direct estimations of the coefficients in relations (1) and (2) from measurements thus avoiding uncertainties of modeling and various assumptions in the range-profiling approaches. Such estimations were the main objective of this study. They take advantage of simultaneous and collocated radar measurements at two frequencies, at one of which attenuation effects in rain are negligible. Direct estimations also allow evaluation of the validity of the linear assumptions in attenuation and deferential attenuation relations.

## 2. Experimental data sources

The dual-wavelength ($\lambda_1 = 3.2$ cm and $\lambda_2 = 11$ cm) radar observations of rainfall used here were performed by the Colorado State University (CSU) CHILL radar during a July - September 2013 project of observing rainfall in the High Park wildfire burn area located west of Fort Collins, CO. The X- and S-band channels of the radar share the same antenna which ensures collocation of beam centers, though the X-band beam is about three times narrower than the 1° wide beam of the S-band channel. The S-band observations are performed in the alternate transmission mode which implies fast switching between horizontal and vertical polarizations. At X-band, a simultaneous transmission – simultaneous receiving (STSR) measurement mode is used. Attenuation and differential attenuation in rain at S-band are more than one order of magnitude smaller than at X-band and can be neglected when estimating X-band attenuation effects from collocated dual-frequency measurements.

Figure 1 shows an example of collocated center beam measurements in the rain during one of the events observed on 18 July 2013. It can be seen that at shorter ranges observed $Z_e$ and $Z_{DR}$ at both frequencies have similar magnitudes but X-band values of these variables get progressively biased low compared to the S-band values as range and the observed X-band differential phase - $\Phi_{DP}$ increase (Fig. 1a). The copolar correlation coefficients $\rho_{hv}$ is rather high (> 0.93) at both frequencies for ranges closer than about 53 km (Fig. 1b). Beyond this range X-band $\rho_{hv}$ drops due to low signal-to-noise ratio as a result of significant attenuation of X-band signals.

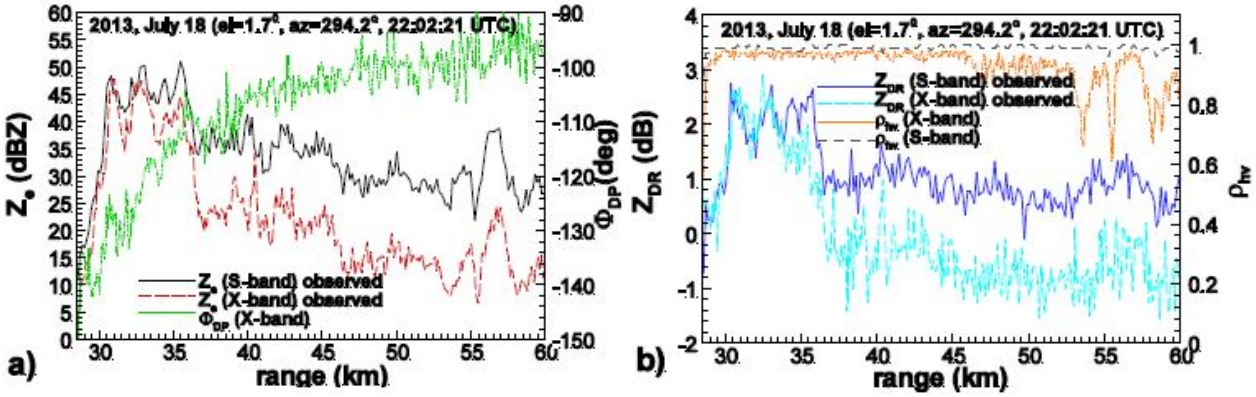


*Figure 1: An example of S- and X-band reflectivity (a) and differential reflectivity (b) measurements along the radar beam (elevation 1.7º, azimuth 294º) observed during the High Park project (2202 UTC, 18 July 2013). Copolar correlation coefficient, $\rho_{hv}$, and X-band differential phase, $\Phi_{DP}(X)$, data are also shown.*

Although most features (e.g., $Z_e$ and $Z_{DR}$ maxima/minima) in Fig.1 are similar at both frequencies, their exact positions sometimes differ slightly which might be a result of differing beam widths and measurement noise. In order to reduce the influence of these factors in further analyses, measurement data were gridded in 1 km cells. During the gridding process, all data points with radar resolution volume centers within a given 1 km cell were averaged in linear scale (e.g., in $mm^6m^{-3}$ units for reflectivity data). An example of such gridding for reflectivity data is depicted in Fig. 2, where the black line shows the beam direction of the data depicted in Fig.1. While such gridding reduces noisiness of the data it is not expected to significantly bias estimations of the relations between attenuation (differential attenuation) and differential phase shift because these relations are quasi-linear.

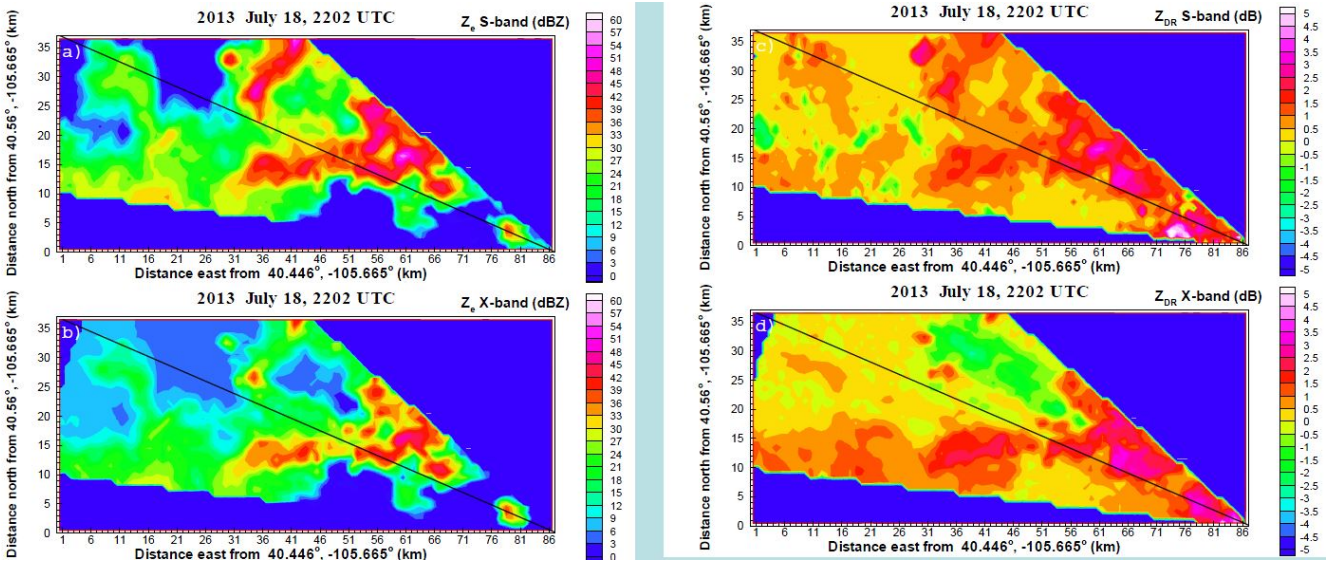


*Figure 2: An example of gridded CHILL dual-wavelength data maps of reflectivity (left) and differential reflectivity (right)*

Overall six experimental events, for which X-band attenuation effects were significant, were observed during the High Park project. The significance of attenuation was judged by the magnitude of X-band differential phase accumulation exceeding a threshold of 30º. A justification for this threshold value is given in the next section. Dual-wavelength reflectivity, differential reflectivity and differential phase data gridding was performed for each of the events. Measurements from the lowest elevation beam tilt that are essentially free of ground clutter (~1.7º) were further used in this study. A typical interval between two consecutive sweeps at this elevation was about 2 min.

### 3. A case study of 18 July 2013

Figure 3 shows scatter plots of gridded X-band differential phase, $\Delta\Phi_{DP}(X)$ and reflectivity and differential reflectivity differences ($\Delta Z$ and $\Delta Z_{DR}$), which were defined as follows

$$\Delta\Phi_{DP}(X) = \Phi_{DP}(X) - 136^o \quad (3)$$
$$\Delta Z = Z_e(S) - Z_e(X) \quad (4)$$
$$\Delta Z_{DR} = Z_{DR}(S) - Z_{DR}(X) \quad (5)$$

where $\Phi_{DP}$(X) - 136° is gridded measured X-band differential phase and 136° is the estimated initial system phase determined by the radar hardware. $\Phi_{DP}$(X) consist of the propagation phase shift $\varphi_{DP}$ and the backscatter phase shift $\delta_{hv}$ at the end of the propagation path:

$$\Phi_{DP}(X) = \varphi_{DP}(X) + \delta_{hv}(X) \quad (6)$$

Since $\varphi_{DP} = \int_0^{r_o} K_{DP}(r)dr$, where the integration is performed over entire propagation path $r_o$, it is the $\varphi_{DP}$(X) contribution to the total phase $\Phi_{DP}$(X) which is related to the total path attenuation and differential attenuation.

The S-band values of $Z_e$(S) and $Z_{DR}$(S) were considered as estimates of nonattenuated reflectivity and differential reflectivity quantities at X-band. Such an assumption for reflectivity is at least justified for $Z_e$(S) < 40 dBZ when typical differences between S- and X-band nonattenuated reflectivities due to higher frequency scattering being outside the Rayleigh regime are generally less than 1 dB or so (Matrosov et al. 2006). Differences between S- and X-band nonattenuated differential reflectivities usually do not exceed 0.3 dB when mean mass-weighted drop diameter does not exceed approximately 2 – 2.5 mm (Matrosov et al. 2006) which approximately corresponds to $Z_{DR}$ values that are less than about 2 dB. A 2 dB $Z_{DR}$ value is also an approximate threshold for which differential phase on backscatter $\delta_{hv}$ can be considered to be less than approximately 3° (e.g., Schneebeli and Berne 2012; Troemel et al. 2013)

The best fit linear (solid lines) and power-law (dashed lines) approximations for the relations $\Delta Z$-$\Delta\Phi_{DP}$(X) and $\Delta Z_{DR}$-$\Delta\Phi_{DP}$(X) are shown in Fig.3. According to the hydrometeor identification scheme performed with weight functions from Dolan and Rutledge (2009) data points overwhelmingly correspond to rainfall. In order to minimize X - S band nonattenuated reflectivity and differential reflectivity differences and influences of backscatter phase shift, these relations were drawn for the subset of data points, which satisfy the threshold conditions: $Z_e$(S) < 40 dBZ, $Z_{DR}$(S) < 2 dB, $\Delta\Phi_{DP}$(X) > 30°, $\rho_{hv}$(X) > 0.9 (even though all data points are shown). The condition $\rho_{hv}$(X) > 0.9 ensures that data points with low SNR and thus not reliable reflectivity estimates (e.g., X-band reflectivity near the end of the radar beam in Fig. 2b) are not used. The condition $\Delta\Phi_{DP}$(X) > 30° is used to minimize possible effects of $\delta_{hv}$ and the noise in differential phase measurements which is typically around 1.5°– 2° (Matrosov et al. 2002).

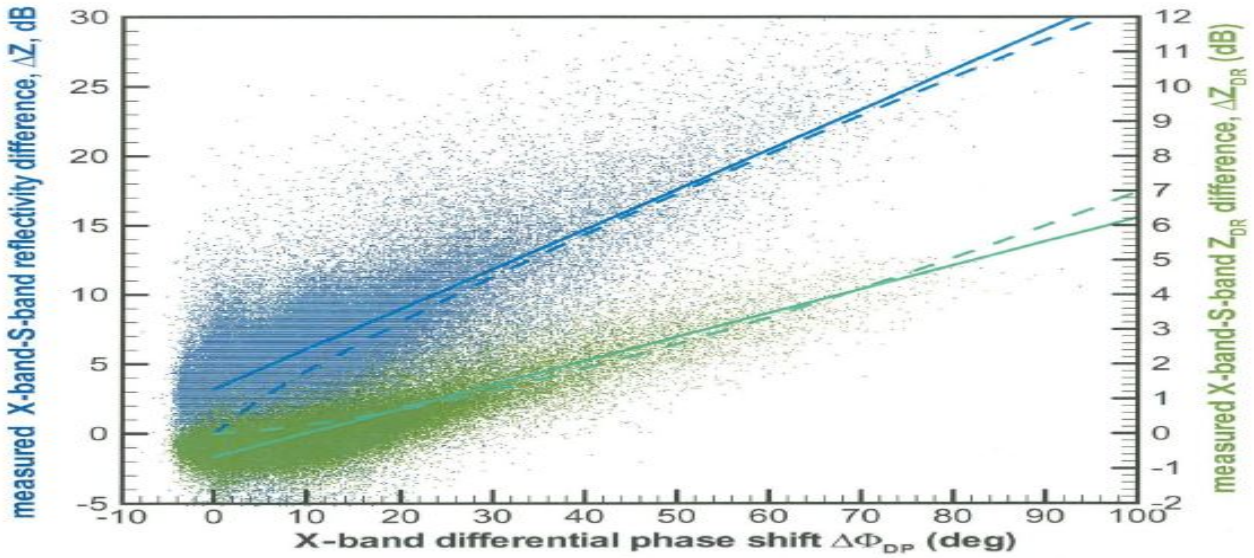


*Figure 3: Scatter plots of measured S-band and X-band reflectivity (blue) and differential reflectivity (green) differences versus measured X-band differential phase for the event of 18 July 2013. Solid (dashed) lines show best linear (power) fir relations for conditions $Z_e$(S) < 40 dBZ, $Z_{DR}$(S) < 2 dB, $\Delta\Phi_{DP}$(X) > 30°, $\rho_{hv}$(X) > 0.9.*

It is seen from Fig.3 that the differences in best linear and power fits are not very significant compared to overall data scatter. This scatter relative to the best fit approximation data amounts to approximately 3.1 dB and 0.6 dB for $\Delta Z$ and $\Delta Z_{DR}$, respectively. Given the close correspondence between linear and power approximations, the linear fits were used hereafter. Under the linear relation assumption and ignoring $\delta_{hv}$, as it is expected to be at least an order of magnitude smaller than propagation phase shift for $\Delta\Phi_{DP}$(X) > 30°, the following expressions for approximations of the can be written

$$\Delta Z = \alpha \cdot \Delta\Phi_{DP}(X) + \Delta Z_0 \quad (7)$$
$$\Delta Z_{DR} = \gamma \cdot \Delta\Phi_{DP}(X) + \Delta Z_{DR0} \quad (8)$$

where coefficients $\alpha$ and $\gamma$ are the same as in (1) and (2). The quantities $\Delta Z_0$ and $\Delta Z_{DR0}$ can be regarded as offsets due to calibration and/or differing radome influences. The values of the coefficients for the event in Fig. 3 are $\alpha$=0.288 dB deg$^{-1}$, and $\gamma$=0.06 dB deg$^{-1}$, correspondingly.

In order to assess the sensitivity of the results to the data gridding procedure, gridding was also performed in the 1 deg and 1 km range intervals (not shown). Since one degree azimuth averaging approximately corresponds to the S-band beam width, three X-band beams were typically averaged to match one beam of S-band data. The derived values of the coefficients $\alpha$ and $\gamma$ for this type of gridding differed from those given above by less than few percent.

## 4. Variability of attenuation – phase relations

All experimental events observed by the CHILL radar during the High Park project, which resulted in significant X-band attenuation effects, were processed in a manner described for the 18 July 2013 case study. The estimated values of the coefficients $\alpha$ (0.252, 0.281, 0.202, 0.270, 0.308, 0.240 dB deg$^{-1}$ for the events of 7/12/2013, 7/18/2013, 7/28/2013 8/3/2013 an 9/12/2013) and $\gamma$ (0.063. 0058, 0.056, 0.065, 0.057, 0.052 dB deg$^{-1}$ for these events) indicate event-to-event variability. The corresponding linear relations are shown in Fig. 4.

Coefficients $\alpha$ obtained here experimentally for $A_h$ - $K_{DP}$ relations agree relatively well with results of theoretical modeling (e.g., Matrosov 2010) which yielded α values between about 0.23 dB deg$^{-1}$ and 0.28 dB deg$^{-1}$ obtained using different drop mean axis ratio models and DSD sets. Experimentally estimated values of $\gamma$ are somewhat higher than theoretical results (~0.04 - 0.05 dB deg$^{-1}$). It cannot be ruled out that some of the differences between experimental and theoretical results may be due to cross-polarization coupling effects that could affect X-band $Z_{DR}$ measurements in the STSR measurement mode. For most of the July-August events precipitation was predominately convective in nature, although relatively short periods of moderate rainfall with a reflectivity bright band, which is characteristic of stratiform-type rain, were present during some of these events as revealed by occasional range-height indicator scans (not shown). No special attempt of separating the results based on the precipitation types was performed because of uncertainties in discriminating local convective-stratiform features on short time scales. All the observed events were relatively warm with similar ground air temperatures of around 15ºC or so. Given this, the temperature dependencies of the coefficients α and γ were not analyzed.

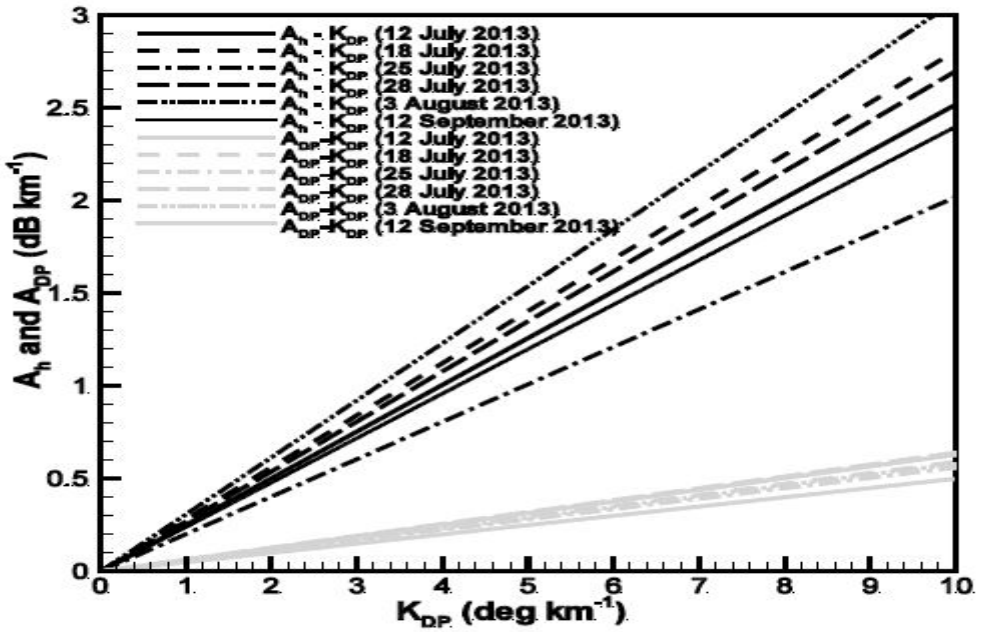


*Figure 4: X-band ( λ= 3.2 cm) attenuation (black lines) and differential attenuation (grey lines) linear correction relations obtained experimentally using data from different events*

One advantage of the approach that was used here for obtaining the coefficients in the linearized $A_h$-$K_{DP}$ and $A_{DP}$-$K_{DP}$ relations is that it is essentially free of modeling assumptions about drop shapes, their oscillation modes, size distributions and a-priori assumptions about the relations about different parameters (e.g., an assumption about a fixed exponent between reflectivity – specific attenuation relations).

## References

Bringi, V.N., and V. Chandrasekar, 2001: *Polarimetric Doppler Weather Radar*. Cambridge University Press, 636 pp.

Bringi, V.N., T.D. Keenan, and V. Chandrasekar, 2001: Correcting C-band radar reflectivity and differential reflectivity data for rain attenuation: A self-Consistent method with constrains. *IEEE Trans. Geosci. Remote Sens*., **39**, 1906-1915.

Dolan, B., and S.A. Rutledge, 2009: A theory-based hydrometeor identification algorithm for X-band polarimetric radars. *J. Atmos. Oceanic Technol*., **26**, 2071-2088.

Matrosov, S.Y., 2010: Evaluating polarimetric X-band radar rainfall estimators during HMT. *J. Atmos. Oceanic. Technol*., **27**, 122-134.

Matrosov, S.Y., K.A. Clark, B.E. Martner, and A. Tokay, 2002: X-band polarimetric radar measurements of rainfall. *J. Appl. Meteorol*., **41**, 941-952.

Matrosov, S.Y., R. Cifelli, P.C. Kennedy, S.W. Nesbitt, S.A. Rutledge, V.N. Bringi, and B.E. Martner, 2006: A comparative study of rainfall retrievals based on specific differential phase shifts at X- and S-band radar frequencies. *J. Atmos. Oceanic Technol.*, **23**, 952-963.

Ryzhkov, A.V., M. Diederich, P. Zhang, and C. Simmer, 2014: Potential utilization of specific attenuation for rainfall estimation, mitigation of partial beam blockage, and radar networking. *J. Atmos. Oceanic Technol*., **31**, 599-619.

Schneebeli, M., and A. Berne, 2012: An extended Kalman filter framework for polarimetric X-band weather radar data processing. *J. Atmos. Oceanic Technol*., **29**, 711-730.

Troemel, S., M.R. Kumjian, A.V., Ryzhkov, C. Simmer, and M. Diederich, 2013: Backscatter differential phase – estimation and variability. *J. Appl. Meteorol. and Climatol*., **52**, 2529-2548.